Oncogene (2005), 1–11

www.nature.com/onc

ORIGINAL ARTICLE

AML1 deletion in adult mice causes splenomegaly and lymphomas

G Putz[1], A Rosner[2], I Nuesslein[1], N Schmitz[1] and F Buchholz[1]

[1]*Max-Planck-Institute for Molecular Cell Biology and Genetics, Pfotenhauerstrasse, Dresden, Germany and* [2]*Klinik und Poliklinik fuer Strahlentherapie und Radioonkologie, Experimentelles Zentrum, Medizinische Fakultaet Carl Gustav Carus, Technische Universitaet Dresden, Fetscherstr., Dresden, Germany*

***AML1* (*RUNX1*) encodes a DNA-binding subunit of the CBF transcription factor family and is required for the establishment of definitive hematopoiesis. *AML1* is one of the most frequently mutated genes associated with human acute leukemia, suggesting that genetic alterations of the gene contribute to leukemogenesis. Here, we report the analysis of mice carrying conditional *AML1* knockout alleles that were inactivated using the Cre/loxP system. *AML1* was deleted in adult mice by inducing Cre activity to replicate *AML1* deletions found in human MDS, familial platelet disorder and rare *de novo* human AML. At a latency of 2 months after induction, the thymus was reduced in size and frequently populated by immature double negative thymocytes, indicating defective T-lymphocyte maturation, resulting in lymphatic diseases with 50% penetrance, including atypical hyperplasia and thymic lymphoma. Metastatic lymphomas to the liver and the meninges were observed. Mice also developed splenomegaly with an expansion of the myeloid compartment. Increased Howell-Jolly body counts indicated splenic hypofunction. Thrombocytopenia occurred due to immaturity of mini-megakaryocytes in the bone marrow. Together with mild lymphocytopenia in the peripheral blood and increased fractions of immature cells in the bone marrow, *AML1* deficient mice display features of a myelodysplastic syndrome, suggesting a preleukemic state.**

Oncogene advance online publication, 10 October 2005; doi:10.1038/sj.onc.1209136

Keywords: AML1; conditional allele; hematopoiesis; splenomegaly; lymphoma

Introduction

The *AML1* gene encodes the acute myeloid leukemia 1 protein (AML1) or Core binding factor alpha 2 subunit (Cbfa2) (Levanon *et al*., 1994). As a master regulatory protein AML1 controls the formation of definitive hematopoietic stem cells (HSCs) (Okuda *et al*., 1996; Wang *et al*., 1996a, b) and is required for the establishment of definitive hematopoiesis (Wang and Speck, 1992; Ogawa *et al*., 1993a; Miller *et al*., 2001) through the regulation of various hematopoietic genes (Rowley, 1998; Roumier *et al*., 2003). Its expression is regulated in a cell-type and maturation-stage specific manner (Lorsbach *et al*., 2004).

AML1 is one of the genes most frequently deregulated in human acute myeloid leukemia through different mechanisms including translocation, mutation and gene amplification (Roumier *et al*., 2003), and is a target for loss of heterozygosity (LOH), suggesting that *AML1* may act as a classical tumor suppressor gene (TSG) (Silva *et al*., 2003). As chromosomal rearrangements are associated with up to 30% of acute leukemias, studies in mice and humans have focussed on the role of translocations in leukemogenesis (Yergeau *et al*., 1997; Okuda *et al*., 1998; Buchholz *et al*., 2000; Rhoades *et al*., 2000; Higuchi *et al*., 2002). Recently, new mechanisms of AML1 deregulation by point mutations or amplification have been reported (Osato *et al*., 1999). Point mutations within the Runt homology domain have been identified as the underlying cause for familial platelet disorder (FPD) with a predisposition to AML, and in rare cases as somatic events of *de novo* AML and myelodysplastic syndromes (Osato *et al*., 1999; Imai *et al*., 2000; Preudhomme *et al*., 2000; Michaud *et al*., 2003; Roumier *et al*., 2003; Taketani *et al*., 2003; Steensma *et al*., 2005). *AML1* point mutations that clustered in the *Runt* domain included silent mutations, heterozygous missense mutations and biallelic nonsense or frameshift mutations (Osato *et al*., 1999).

The effect of AML1 deregulation by *AML1* mutations has also been studied in transgenic mouse models. Homozygous deletion of either *AML1* or *CBF* results in embryonic lethality. $AML1^{-/-}$ embryos die from an absence of definitive hematopoiesis, central nervous system hemorrhages and necrosis (Okuda *et al*., 1996; Wang *et al*., 1996a; North *et al*., 1999). Haploinsufficiency of AML1 causes an autosomal dominant congenital platelet defect due to defective megakaryopoiesis and predisposes to the acquisition of additional mutations resulting in leukemia (Song *et al*., 1999; Sun and Downing, 2004).

Embryonic lethality of $AML1^{-/-}$ mutant mice makes it impossible to study the function of *AML1* in the adult organism. Only recently this problem has been addressed by two studies generating mice with conditional

Correspondence: Dr F Buchholz, MPI-CBG, Pfotenhauer Str. 108, 01307 Dresden, Germany.
E-mail: buchholz@mpi-cbg.de
Received 24 March 2005; revised 6 July 2005; accepted 23 August 2005

AML1 knockout alleles under the control of different promoters (Taniuchi *et al*., 2002; Ichikawa *et al*., 2004). The *AML1* knockout in early T-cell progenitors by use of the *lck* promoter showed that AML1 is required for *CD4* silencing in double-negative (DN) $CD4^-CD8^-$ thymocytes, for β selection of DN thymocytes, and CD8 upregulation (Taniuchi *et al*., 2002). Ichikawa *et al*. (2004) reported a conditional knockout of *AML1* in transgenic *Mx-Cre* mice, providing Cre activity after induction in a wide range of hematopoietic cells. In this study, mice lacking *AML1* only showed minor effects on hematopoiesis, including a reduced number of platelets and mature lymphocytes in the peripheral blood, suggesting that AML1 is necessary for the proper maturation of lymphocytes and megakaryocytes, but dispensable for other myeloid lineage cells. An expansion and altered *in vitro* growth characteristics of the myeloid progenitor population were observed, as well as an expansion of the most immature progenitor population in the BM, indicating either a larger pool of stem cells, or an inhibition of their differentiation. For the maintenance of HSCs, *AML1* was not necessary. However, structural and functional defects of hematopoietic organs were not reported.

Here, we report the generation of mice carrying a loxP-flanked exon 5 of the *AML1* gene ($AML1^{fl/fl}$). The usage of the interferon-responsive *Mx*-promoter for site-specific recombination at the loxP sites enabled us to efficiently delete exon 5 in the hematopoietic system of adult mice by treatment of the mice with PolyIPolyC. In contrast to Ichikawa *et al*. (2004), our study concentrates on the progression of the phenotype at later time-points after the induction of the *AML1* deletion. About 2 months after PolyIPolyC treatment, we observed a striking phenotype in *Mx-Cre* excised *AML1* ($AML1^{\Delta/\Delta}$) mice including progressive splenomegaly with an expansion of the myeloid compartment at the expense of the white pulp and signs of splenic hypofunction. Together with cytopenia in the peripheral blood and increased fractions of immature cells in the BM, we observed features of a myelodysplastic syndrome, suggesting a preleukemic state. Thymus size was reduced with a frequent shift of the thymocyte populations towards the very immature DN $CD4^-CD8^-$ fraction. In some $AML1^{\Delta/\Delta}$ mice, we observed the development of thymic atypical hyperplasia or metastatic lymphoma. Therefore, our study shows that the lack of AML1 severely affects the structure and function of hematopoietic organs.

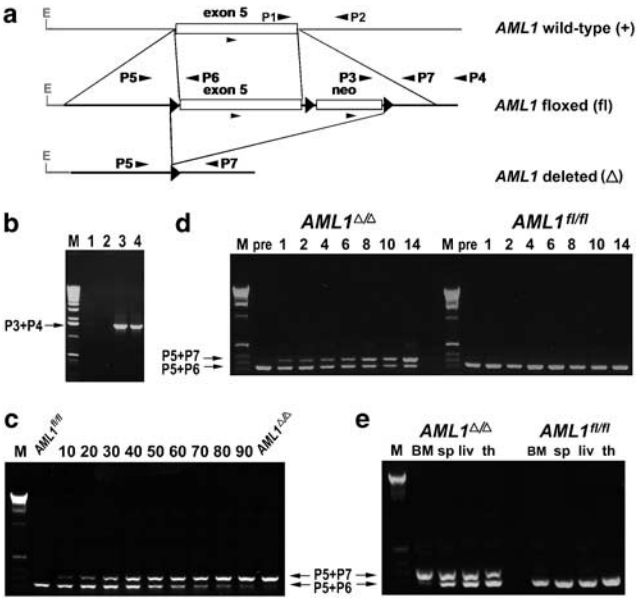

Figure 1 Genotyping of the targeting construct in $AML1^{fl/fl}$ and $AML1^{\Delta/\Delta}$ mice. (**a**) Scheme for induction of homologous recombination by Cre recombinase including loxP sites (triangle), neomycin cassette (neo), and annealing point of primers for PCR. Scheme shows the *AML1* wild-type allele (top), the *AML1* targeting construct before (middle, floxed (fl)) and after Cre-mediated site-specific recombination of the loxP cassette (bottom, deleted(Δ)) due to treatment with the interferon-inducer PolyIPolyC. Recombination of the loxP cassette results in deletion of exon 5 of the murine *AML1* gene. (**b**) Genotyping of ES cell clones. Result of PCR using primers P3 + P4 with clones #1 and 2 (negative) and clones #3 and 4 (positive) are shown. (**c–e**) Genotyping of cells from hematopoietic organs after injection of mice with the PolyIPolyC. Triple-primer PCR reactions were performed with primers P5 + P6 + P7 (see Table 1, Supplement). Cre-mediated deletion of exon 5 results in a 382 bp band (P5 and P7), while a 325 bp band is expected before recombination (P5 and P6). (**c**) Triple-primer PCR with dilution series of template DNA. DNA was isolated from the BM of an $AML1^{\Delta/\Delta}$ mouse and a control mouse 107 days after PolyIPolyC injection. Template of first lane contains only DNA of the control mouse, while template of last lane contains only DNA of the $AML1^{\Delta/\Delta}$ mouse. Lanes 2–10 show templates of mixtures with different proportions of control DNA vs DNA of the $AML1^{\Delta/\Delta}$ mouse. Numbers indicate the percentage of DNA of the $AML1^{\Delta/\Delta}$ mouse in the template mixture (10–90%). DNA concentrations of all template mixtures were equal. (**d**) Cre-mediated recombination of exon 5 in the peripheral blood of $AML1^{\Delta/\Delta}$ (left) and $AML1^{fl/fl}$ mice (right) at different time-points (in weeks) after injection of PolyIPolyC (pre = prior to PolyIPolyC injection). (**e**) Figure shows recombination in the bone marrow (BM), spleen (sp), liver (liv) and thymus (th) of $AML1^{\Delta/\Delta}$ (left) and control mice (right) 107 days after PolyIPolyC treatment.

Results

Generation of mice carrying loxP sites in introns of the AML1 *gene*

To study the function of the murine *AML1* gene in adult mice, we generated mice with an *AML1* targeting construct (Figure 1a). The floxed exon 5 contains part of the runt homology domain responsible for heterodimerization with the beta subunit and DNA binding (Ogawa *et al*., 1993b; Wang *et al*., 1996b). Since a C-terminal truncation of AML1 is sufficient to disrupt DNA-binding and heterodimerization with CBFb (Lenny *et al*., 1995), and partial loss of the runt domain (aa 143–178) destroys the ability of AML1 to bind DNA and heterodimerize with the CBFb subunit (Wang *et al*., 1996a), deletion of exon 5 is expected to result in a functional *AML1* knockout.

To evaluate recombination efficiency after PolyIPolyC treatment, we established a triple-primer PCR assay with primers annealing to the *AML1* gene (Figure 1a, primers P5 + P6 + P7). In the targeted *AML1* alleles we

expect a 325 bp band as a PCR product of primers P5 and P6. PCR cycles were chosen such that a PCR product of primers flanking exon 5 (P5 and P7) with an expected length of 5.5 kb was not amplified. After the deletion of exon 5 a band of 382 bp is obtained (P5 and P7) due to the remaining sequence of a loxP site (34 bp) in the intron (348 bp). Recombination efficiency larger than 0%, but less than 100% results in two DNA bands, a 325 bp and a 382 bp band. To test whether the relation of band strength reflects recombination efficiency, we performed PCRs using a dilution series of nonrecombined DNA from the BM of a control mouse and recombined DNA from the BM of an *AML1*$^{\Delta/\Delta}$ mouse as a template (Figure 1c). The intensity of the 382 bp band increases with the amount of recombined DNA in the reaction. The ratio of the band intensities can be used to determine the approximate recombination efficiency. Analysis of Cre-mediated recombination in the peripheral blood of *AML1*$^{\Delta/\Delta}$ mice showed that recombination increased over time (Figure 1d), indicating that *AML1*$^{\Delta/\Delta}$ cells have a survival advantage over *AML1*$^{fl/fl}$ cells. We, then, tested the efficiency of recombination in different organs (Figure 1e). Recombination was strongest in the BM, followed by spleen, liver and thymus. Before PolyIPolyC treatment, no recombination was detectable (Figure 1d, lane pre), confirming that Cre recombinase is not expressed in untreated mice. Heterozygous *AML1*$^{fl/+}$ and homozygous *AML1*$^{fl/fl}$ mice were viable with no obvious anatomical or behavioral defects.

Adult AML1$^{\Delta/\Delta}$ *mice develop thrombocytopenia*

Complete blood cell counts were performed weekly after PolyIPolyC injections. Already one week after the first injection (PolyIPolyC was injected three times in two-day intervals), the number of thrombocytes in the peripheral blood of *AML1*$^{\Delta/\Delta}$ mice had significantly decreased compared to *AML1*$^{fl/fl}$ control mice (Figure 2a, *t*-test, 1st week: $P<0.05$; 2nd–6th week: $P<0.01$). Investigations of the BM of *AML1*$^{\Delta/\Delta}$ mice revealed the presence of megakaryocytes, which were reduced in number and size (so called 'micromegakaryocytes'). May-Grünwald/Giemsa-stainings confirmed the reduction of thrombocytes and occasionally revealed the presence of Howell-Jolly bodies in peripheral blood smears (Figure 2b). Red blood cells containing Howell-Jolly bodies indicate an impaired clearance by the splenic vascular system (Morohashi *et al*., 1999). More than 2 months after PolyIPolyC injection, 0.51% of the erythrocytes of *AML1*$^{\Delta/\Delta}$ mice contained Howell-Jolly bodies compared to 0.16% in control mice ($n_{AML1fl/f}=6$, $n_{AML1\Delta/\Delta}=6$; *t*-test: $P<0.001$), suggesting impaired splenic function.

White blood cell (WBC) counts varied, with no dramatic increase in numbers observed within 4 months after the deletion of exon 5 of *AML1*. In contrast, number of lymphocytes were reduced in *AML1*$^{\Delta/\Delta}$ mice 4 weeks after the first PolyIPolyC injection (Figure 2c, *t*-test, 3rd–4th week: $P<0.01$; 5th week: $P<0.05$, 6th week: $P<0.01$). The number of monocytes, granulocytes, erythrocytes and the hemoglobin level of *AML1*$^{\Delta/\Delta}$ mice were not affected (data not shown). Pappenheim method (May-Grünwald/Giemsa-stain), Peroxidase stains, and Alpha-naphthyl acetate esterase stains of peripheral blood smears showed no obvious number of blast cells, but differentiated cells of all types of WBCs (data not shown). Thus, deletion of *AML1* in adult mice had no dramatic effect on cellularity in the peripheral blood, except for thrombocytopenia and moderate lymphocytopenia.

AML1$^{\Delta/\Delta}$ *mice develop splenomegaly and lymphomas*

Pathological analysis revealed that *AML1*$^{\Delta/\Delta}$ mice develop splenomegaly (Figure 2d). During the first 7 weeks after injection of PolyIPolyC, an increase in spleen size was only observed sporadically with no statistically significant difference between *AML1*$^{\Delta/\Delta}$ and control mice ($n_{AML1fl/fl}=4$, $n_{AML1\Delta/\Delta}=5$, *t*-test: p = n.s.). More than 7 weeks after PolyIPolyC treatment, however, the increase of spleen weight in *AML1*$^{\Delta/\Delta}$ mice was highly significant, with spleen body weight ratios up to 0.010 (see Table 1), suggesting that a progression of splenomegaly positively correlated with the time span of the induced deletion ($n_{AML1fl/fl}=31$, $n_{AML1\Delta/\Delta}=28$; *t*-test: $P<0.001$; Figure 2d).

Analysis of the spleen architecture showed a reduced and dispersed white pulp with a striking expansion of the red pulp compartment in *AML1*$^{\Delta/\Delta}$ mice (Figure 2e). Immunostainings of spleen tissue with B-cell marker B220 (Figure 3a and b) and T-cell marker CD4 (Figure 3c and d) revealed a reduction of the lymphocyte populations in the white pulp, confirming results from hematoxylin eosin stains (Figure 2e), while myeloid markers anti-CD11b (Figure 3e and f) and anti-Gr-1 (Figure 3g and h) showed an increase in the myeloid cell population in the red pulp of *AML1*$^{\Delta/\Delta}$ mice. To quantify shifts in granulocyte and monocyte/macrophage cell populations, we performed FACS analysis of murine spleen cells two months after PolyIPolyC injection (Figure 4). Increased numbers of cells stained positively for the myeloid markers Gr-1 (Figure 4a, *AML1*$^{\Delta/\Delta}$ 28.0% vs *AML1*$^{fl/fl}$ 11.8%) and CD11b (Figure 4b, *AML1*$^{\Delta/\Delta}$ 32.3% vs *AML1*$^{fl/fl}$ 11.1%) in *AML1*$^{\Delta/\Delta}$ mice. More detailed analyses of the myeloid cell fraction revealed an enlarged population of neutrophil Gr-l^{hi}/CD11b^{lo-hi} cells (P1, *AML1*$^{\Delta/\Delta}$ 18.4% vs *AML1*$^{fl/fl}$ 3.9%) and Gr-1 $^{neg-lo}$/CD11b^{hi} monocyte lineage cells (P2, *AML1*$^{\Delta/\Delta}$ 9.8% vs *AML1*$^{fl/fl}$ 1.8%) in *AML1*$^{\Delta/\Delta}$ mice (Figure 4c). Genotyping of the two cell populations after cell sorting showed full recombination (Figure 4l), suggesting increased number of myeloid cells as a consequence of the *AML1* deficiency. The increase might be due to the accumulation of immature neutrophils and myelomonocytes observed in the Gr-1^{lo-hi}/CD11b^{lo-hi} cell fraction (Lagasse and Weissman, 1996). As the numbers of granulocytes and monocytes in the peripheral blood of *AML1*$^{\Delta/\Delta}$ mice did not differ from control mice, the accumulation of immature myelomonocytic cells appear to result from an enlarged pool of myeloid progenitors, but not from a

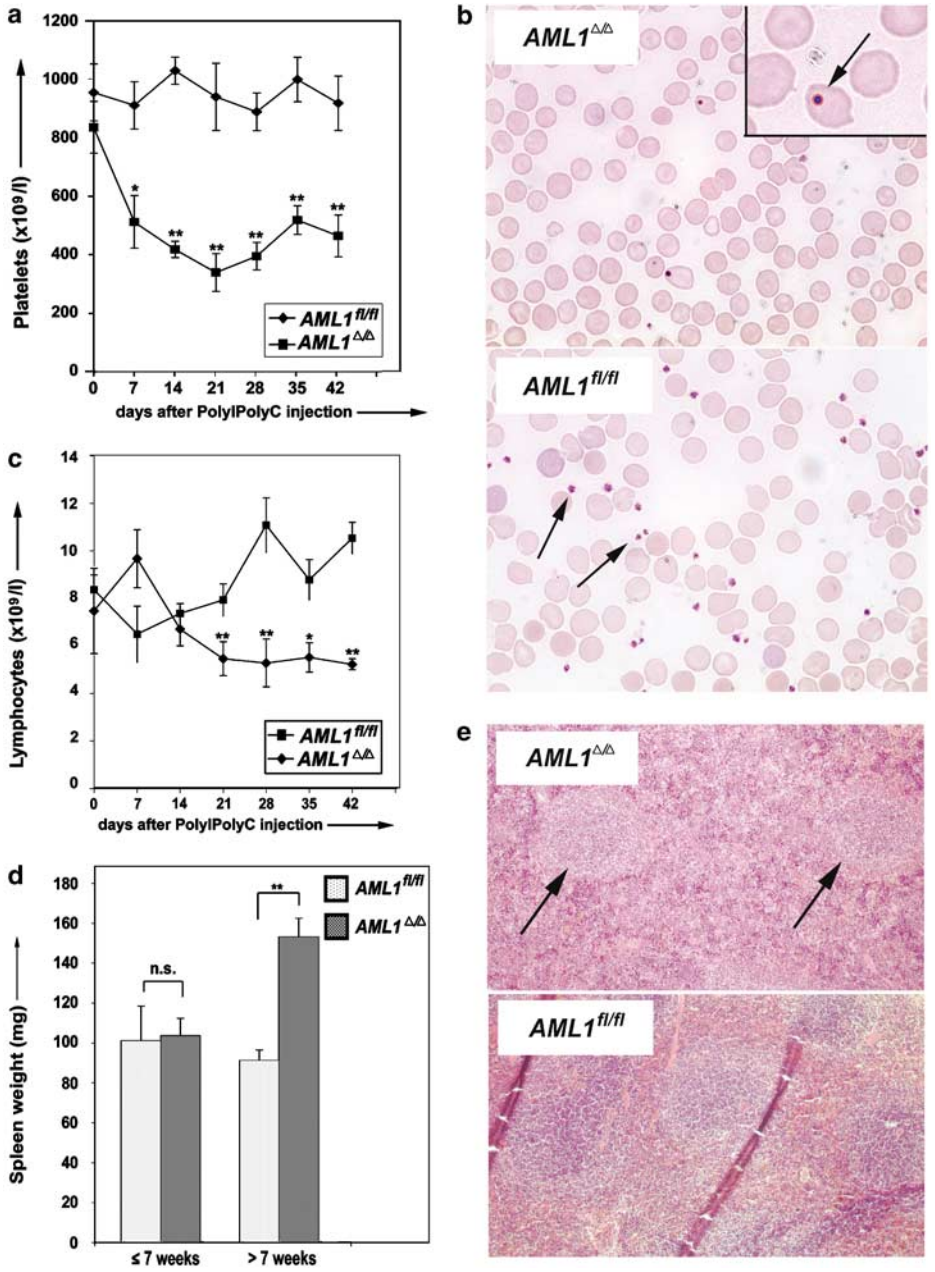

Figure 2 Pathology of the peripheral blood and spleen of *AML1*$^{\Delta/\Delta}$ mice. **(a)** Results of platelet counts of peripheral blood of *AML1*$^{\Delta/\Delta}$ and control mice. Figure shows the average numbers of thrombocytes (10^9/l) of four mice per group. **(b)** Pappenheim's stain (May-Grünwald/Giemsa-stain) of peripheral blood smear. Arrows indicate platelets in the control. Inset in figure of *AML1*$^{\Delta/\Delta}$ mouse shows erythocyte with Howell-Jolly body (arrow) at higher magnification. **(c)** Results of lymphocyte counts of the peripheral blood of *AML1*$^{\Delta/\Delta}$ and control mice. Figure shows the average numbers of lymphocytes (10^9/l) of four mice per group. **(d)** Development of spleen weight after injection of PolyIPolyC. Mean of spleen weight of *AML1*$^{\Delta/\Delta}$ vs control mice up to 7 weeks after PolyIPolyC treatment (left bars, p = n.s.) and more than 7 weeks after induction of Cre recombinase (right bars, *t*-test: $P<0.001$). **(e)** Spleen histology of *AML1*$^{\Delta/\Delta}$ and *AML1*$^{fl/fl}$ mice, H&E stain, original magnification $\times 100$. Arrows indicate the largely scattered white pulp in *AML1*$^{\Delta/\Delta}$ mice.

block in myeloid differentiation. Results from double staining of splenic cells with stem cell and progenitor markers c-Kit (CD117) and Sca-1 (Ly6A/E) confirm this hypothesis, as the Sca-1$^-$ c-Kit$^+$ fraction including myeloid progenitors (Figure 4d, P2, *AML1*$^{\Delta/\Delta}$ 6.0% vs *AML1*$^{fl/fl}$ 1.4%) and the Sca-1$^+$ c-Kit$^+$ cell population enriched with HSCs were enlarged in *AML1*$^{\Delta/\Delta}$ mice (Figure 4d, P1, *AML1*$^{\Delta/\Delta}$ 2.9% vs *AML1*$^{fl/fl}$ 1.5%). Similar results were obtained for Prominin-1 (Yin *et al*., 1997), which is expressed on primitive cells such as hematopoietic stem and progenitor cells, neural and endothelial stem cells, retina and retinoblastoma, as well as developing epithelium (Figure 4e, *AML1*$^{\Delta/\Delta}$ 12.2% vs *AML1*$^{fl/fl}$ 5.3%). Splenomegaly, therefore, appears to result from increased extramedullary hematopoiesis in the spleen, which leads to an expansion of the red pulp

Table 1 Parameters of *AML1*$^{fl/fl}$ and *AML1*$^{\Delta/\Delta}$ mice

Latency day	*Mouse no.*	*AML1*$^{fl/fl}$				*AML1*$^{\Delta/\Delta}$				
		Spleen mg	*Body g*	*Ratio*	*Figure*	*Mouse no.*	*Spleen mg*	*Body g*	*Ratio*	*Figure*
23	m2411	87.2	56.0	0.002		m2412	102.3	29.0	0.004	
38	m2691	93.8	31.6	0.003	4k	m2756	103.6	32.6	0.003	4k
42	f2753	150.1	23.4	0.006		f2758	75.0	24.4	0.003	
45	m2755	71.2	29.9	0.002		f2760	105.4	24.8	0.004	
46						f2751	129.1	22.0	0.006	
59	m2825	61.1	24.8	0.002		m2836	125.8	32.8	0.004	
65	f2757	78.6	23.7	0.003	4a–c,e	f2771	159.1	22.6	0.007	4a–c,e
66	f2759	58.9	22.1	0.003		f2772	167.1	24.5	0.007	
72	m2769	116.9	40.6	0.003		m2787	108.0	25.9	0.004	
73	m2770	85.3	34.7	0.002		m2823	97.0	36.7	0.003	
81	m2571	105.9	ND	ND		f2663	192.1	ND	ND	
98	f2746	76.7	21.9	0.004	2e; 3	f2745	222.2	27.0	0.008	2e; 3; 5e,f
98	f2752	178.4	23.4	0.008		f2754	241.8	25.4	0.010	5d
103	m3053	66.4	31.3	0.002						
103	f3055	76.6	23.1	0.003		m3061	109.2	27.0	0.004	
103	m3058	101.9	37.6	0.003						
107	m2886	84.3	30.5	0.003	Sup b	f2935	144.6	20.8	0.007	Sup c–d
108	f2573	69.6	ND	ND	2b	m2583	176.0	ND	ND	2b
113	f2887	110.3	25.8	0.004	Sup a	m2956	169.4	31.1	0.005	5g–j; Sup e–f
118	m3062	98.0	28.9	0.003		m3080	198.2	44.6	0.004	
188	f3069	87.2	25.7	0.003		m3082	114.3	27.0	0.004	
128	f2826	49.0	19.3	0.003	5a	m2839	101.2	22.9	0.004	5a
128	f2888	137.9	35.0	0.004		m2964	114.9	29.5	0.004	
128	f2889	91.1	31.8	0.003		m2987	81.9	29.5	0.003	
134	f2827	87.3	29.6	0.003		m2852	134.8	39.4	0.003	
135	f2906	66.0	28.2	0.002	4f–i	m2989	205.7	29.3	0.007	4f–i
136	m2829	113.8	44.2	0.003		m2930	263.4	33.9	0.008	
136	m2828	152.9	33.8	0.005	5c					
143	f2831	86.1	29.6	0.003	4d	m2953	119.2	27.2	0.004	4d
148	f2890	86.3	26.6	0.003		f2992	197.9	24.6	0.008	
148	f2891	86.8	32.2	0.003		m3002	200.7	30.7	0.007	
149	m2885	103.3	31.0	0.003	4j	m2954	160.9	40.4	0.004	4j
155	f2577	69.6	20.8	0.003						
162	m2907	47.9	23.2	0.002		f3005	150.5	22.6	0.007	
198	f2832	71.1	33.1	0.002		m2900	102.2	23.7	0.004	
199	f3078	106.8	25.2	0.004		m2955	114.3	25.0	0.005	
199						f2909	85.3	24.1	0.004	

Table shows number of days between PolyIPolyC injection and preparation (Latency day), identification number of mouse (Mouse no.), spleen weight (Spleen), body weight (Body), body weight ratio (Ratio), and mice shown in figures in the text (Figure); ND = not determined; Sup = Supplementary figure.

compartment by an accumulation of HSCs and immature myeloid lineage cells. Focal extramedullary hematopoiesis was also increased in the liver of *AML1*$^{\Delta/\Delta}$ mice (see Figure in the Supplementary Materials link). Besides the described cell populations, lymphocytes and mini-megakaryocytes, increased numbers of mast cells were found within the red pulp of the *AML1*$^{\Delta/\Delta}$ mice. Goldner's staining failed to show increased fibrosis of the spleen, and vascular neoplasms were excluded by immunofluorescence for CD31 (data not shown). This along with normal hemoglobin values and erythrocyte counts suggests that the observed functional hyposplenism is due to an immaturity of the macrophages.

In contrast, the relative numbers of B-cells in the spleen were found to be reduced in *AML1*$^{\Delta/\Delta}$ mice (Figure 4f, B220: *AML1*$^{\Delta/\Delta}$ 22.3% vs *AML1*$^{fl/fl}$ 39.2%) and explain the reduced size of the white pulp (Figure 3). More detailed analysis showed that the proportion of mature IgM$^+$B220$^+$ cells was reduced (Figure 4g, *AML1*$^{\Delta/\Delta}$ 15.1% vs *AML1*$^{fl/fl}$ 23.6%), while the population of immature IgM$^-$B220^{lo} cells was comparable to that in control mice (Figure 4g, *AML1*$^{\Delta/\Delta}$ 2.1% vs *AML1*$^{fl/fl}$ 1.5%), indicating defective maturation of B-lymphoid cells. Additionally, we observed a relative decrease of the T-cell population in the spleen of mice lacking AML1 (Figure 4h, *AML1*$^{\Delta/\Delta}$ 23.3% vs *AML1*$^{fl/fl}$ 48.0%). A closer look at the lymphoid population using their forward and side scatter parameters, revealed a relatively enlarged population of DN CD4$^-$CD8$^-$ cells in *AML1*$^{\Delta/\Delta}$ mice (Figure 4i, *AML1*$^{\Delta/\Delta}$ 67.3% vs *AML1*$^{fl/fl}$ 46.4%), which could be either B-lymphocytes, or very immature T-lymphocytes. As the B-lymphoid cell population was not enlarged in *AML1*$^{\Delta/\Delta}$ mice (Figure 4f), we conclude that very immature T-lympocytes contribute to the increase of the DN CD4$^-$CD8$^-$ cells, indicating a block in T-cell maturation.

To study whether a block in T-cell maturation is also observed in the thymus, we investigated structure and cellularity of this organ. Most *AML1*$^{\Delta/\Delta}$ mice appeared to have smaller thymuses than control mice (Figure 5a

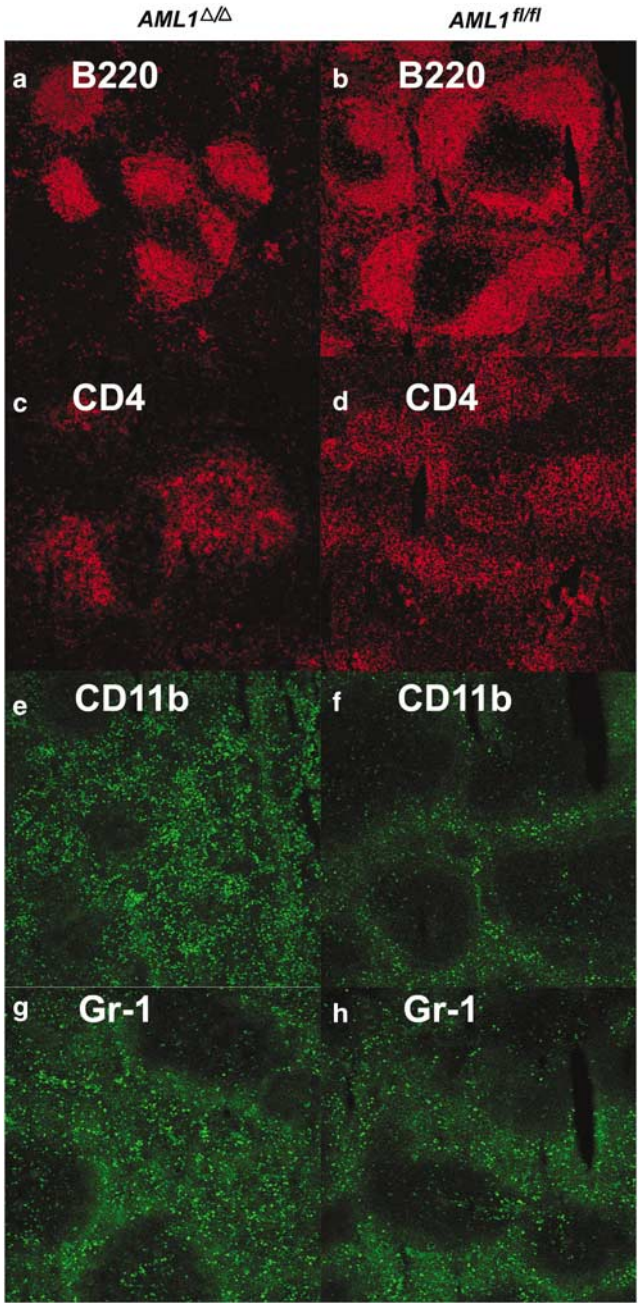

Figure 3 Immunofluorescence analyses of spleen in *AML1*$^{\Delta/\Delta}$ and *AML1*$^{fl/fl}$ mice. Spleen tissue sections stained with antibodies specific for anti-B220 (CD45R, **a**, **b**), anti-CD4 (L3T4, **c**, **d**), anti-CD11b (Mac1, **e**, **f**), and anti-Gr-1 (Ly6G, **g**, **h**), original magnification $\times 100$. **a-d**: Dispersed and reduced white pulp in *AML1*$^{\Delta/\Delta}$mice. The splenic follicles have a reduction of mature T lymphocytes, which form the periarteriolar lymphoid sheath (PALS) seen as negative centers in (**a**). **e–h**: Staining with anti-Gr1 (Ly6G) and anti-CD11b (Mac1) show an enlarged red pulp in *AML1*$^{\Delta/\Delta}$mice with an enrichment of myeloid cells (**g**), and infiltration of the white pulp by macrophages (**e**).

and b), which was also reflected in reduced thymus weight of 42.0 ± 5 mg compared to 73.9 ± 8 mg in control mice ($n_{AML1fl/fl} = 13$, $n_{AML1\Delta/\Delta} = 14$; *t*-test: $P < 0.01$). FACS analysis with antibodies specific for T-lymphocyte development showed a markedly enlarged population of immature DN thymocytes in six out of 12 investigated *AML1*$^{\Delta/\Delta}$ mice (Figure 4j, *AML1*$^{\Delta/\Delta}$ 97.1% vs *AML1*$^{fl/fl}$ 17.2%), while the DP population (Figure 4j, *AML1*$^{\Delta/\Delta}$ 0.8% vs *AML1*$^{fl/fl}$ 76.7%), as well as the SP CD4$^+$CD8$^-$ (Figure 4j, *AML1*$^{\Delta/\Delta}$ 0.9% vs *AML1*$^{fl/fl}$ 3.8%) and CD4$^-$CD8$^+$ cell populations (Figure 4j, *AML1*$^{\Delta/\Delta}$ 1.2% vs *AML1*$^{fl/fl}$ 2.4%) were strongly reduced. In *AML1*$^{\Delta/\Delta}$ mice with a reduced thymus, the overall number of thymic cells was severely reduced. These results confirm a block in T-cell maturation in the thymus, and may explain lymphocytopenia in the peripheral blood.

At histological examination, the distinction between thymic medulla and cortex was lost in two of the six *AML1*$^{\Delta/\Delta}$ mice studied (Figure 5c–e). In both mice, the medulla was populated by immature lymphoblasts at 98 days after PolyIPolyC treatment. In one case this was confined to the thymus (Figure 5d). This along with a small size of the affected thymic lobe has previously been reported as atypical hyperplasia in chemically induced lymphoma (Dunnick *et al*., 1997). In the other case, lymphoblasts expanded beyond the thymic capsule (Figure 5e and f) and metastasized to the liver, representing a metastatic thymic lymphoma. Another mouse had histological evidence of a malignant lymphoma of a cervical lymph node metastatic to the brain (Figure 5g–j). Described lymphomas were negative for B-cell marker B220, and are therefore assumed to be T-cell lymphomas (data not shown). No lymphomas were found in age- and induction-matched control mice. In mice without lymphoid neoplasms, the secondary follicles in peripheral lymph nodes and Peyer's patches of *AML1*$^{\Delta/\Delta}$ mice were either very small compared to the *AML1*$^{fl/fl}$ mice, or completely missing. This might indicate a reduced activation of B lymphocytes in absence of mature T lymphocytes.

To analyse whether the partial deletion of the *AML1* gene affects cellularity in the BM, FACS analysis was performed. We observed a eight-fold increase of the Sca-1$^+$ c-Kit$^+$ population in the total BM of *AML1* excised animals compared to control mice (data not shown). Flow cytometry analysis of lineage-negative depleted BM cells revealed an increased fraction of HSCs (Figure 4k, P1, Sca-1$^+$ c-Kit$^+$: 11.7% in *AML1*$^{\Delta/\Delta}$ vs 6.4% in *AML1*$^{fl/fl}$ mice) and myeloid progenitors (Figure 4k, P2, Sca-1$^-$ c-Kit$^+$: 34.5% in *AML1*$^{\Delta/\Delta}$ vs 23.9% in *AML1*$^{fl/fl}$ mice) 5 weeks after injection of PolyIPolyC, which indicated either increased proliferation of hematopoietic stem and progenitor cells or a block in the maturation of hematopoietic progenitors.

Discussion

The *AML1* gene is one of the most frequently mutated genes in human leukemias. Investigation of *AML1* mutations in transgenic mouse models, therefore, might help to understand the role of AML1 in hematopoiesis and its leukemogenic potential. The inducible deletion of *AML1* in adult mice enabled us to

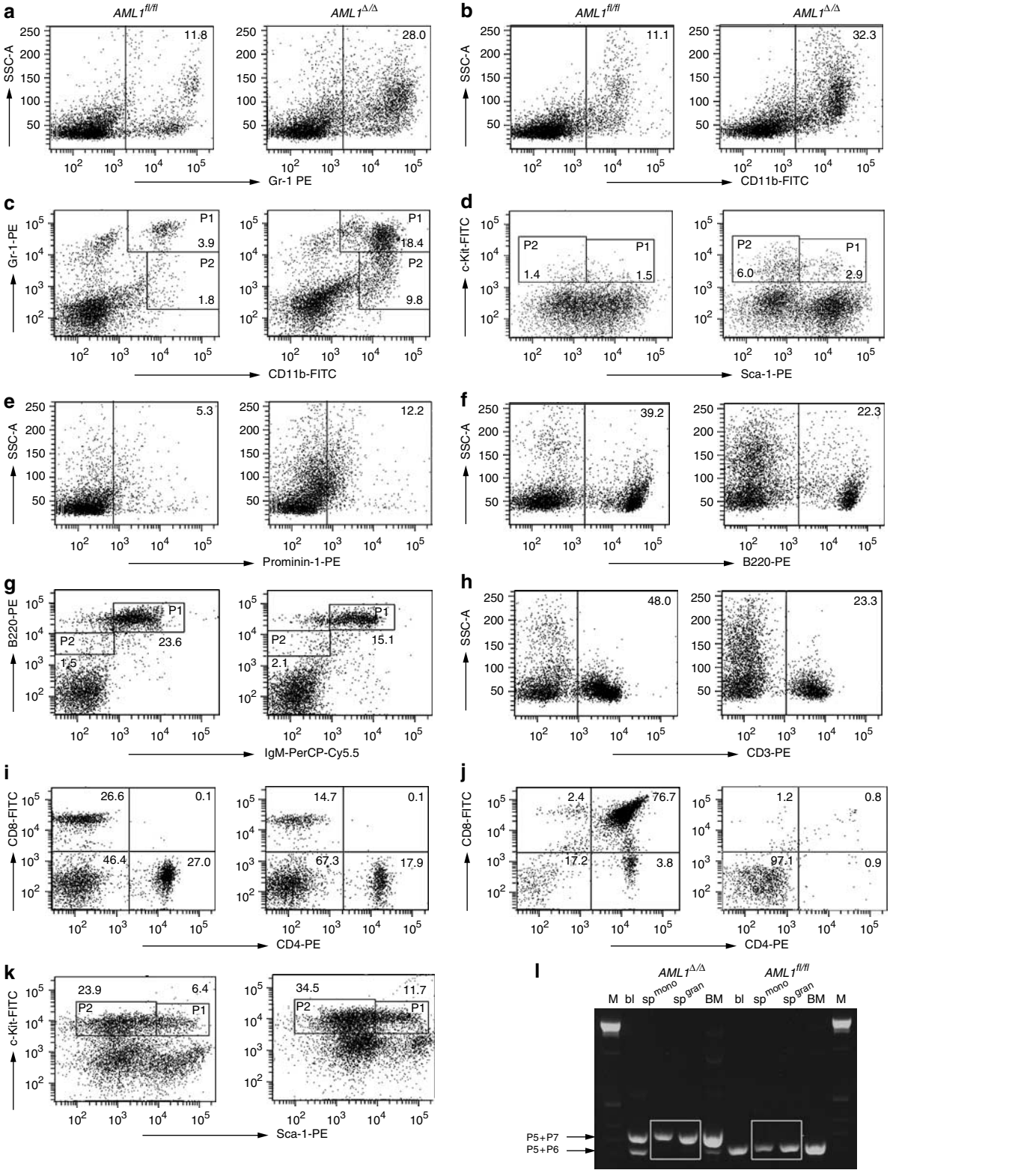

Figure 4 Flow cytometry analysis of spleen, thymus and BM cells of *AML1*$^{fl/fl}$ and *AML1*$^{\Delta/\Delta}$ mice. **(a–i)** FACS analyses of spleen cells. Spleen cells were stained with rat anti-mouse Gr-1 (**a**), CD11b (**b**), double stained with Gr-1 and CD11b (**c**), c-Kit and Sca-1 (**d**), Prominin-1 (**e**), B220 (**f**), B220 and IgM (**g**), CD3 (**h**), CD4 and CD8 (**i**). (**j**) FACS analyses of thymic cells. Cells were double stained with CD4 and CD8. (**k**) FACS analyses of BM cells. Figures show results of double staining of lineage negative depleted (lin$^-$) BM cells with Sca-1 and c-Kit. (**l**) Splenic monocytes and granulocytes were sorted after double staining with Gr-1 and CD11b. Figure shows result of genotyping of peripheral blood cells (bl), splenic monocytes (mono) and splenic granulocytes (gran) of an *AML1*$^{\Delta/\Delta}$ mouse. Triple-primer PCR reactions were performed with primers P5 + P6 + P7 (see Table 1, Supplement).

circumvent embryonic lethality and to recapitulate the situation found in human cancers where mutations are believed to occur during later stages of development.

In the first weeks after deletion of *AML1*, we observed a mild phenotype including thrombocytopenia and slight lymphocytopenia in the peripheral blood, together with an expansion of progenitor populations in the BM, supporting the idea that *AML1* is essential for the

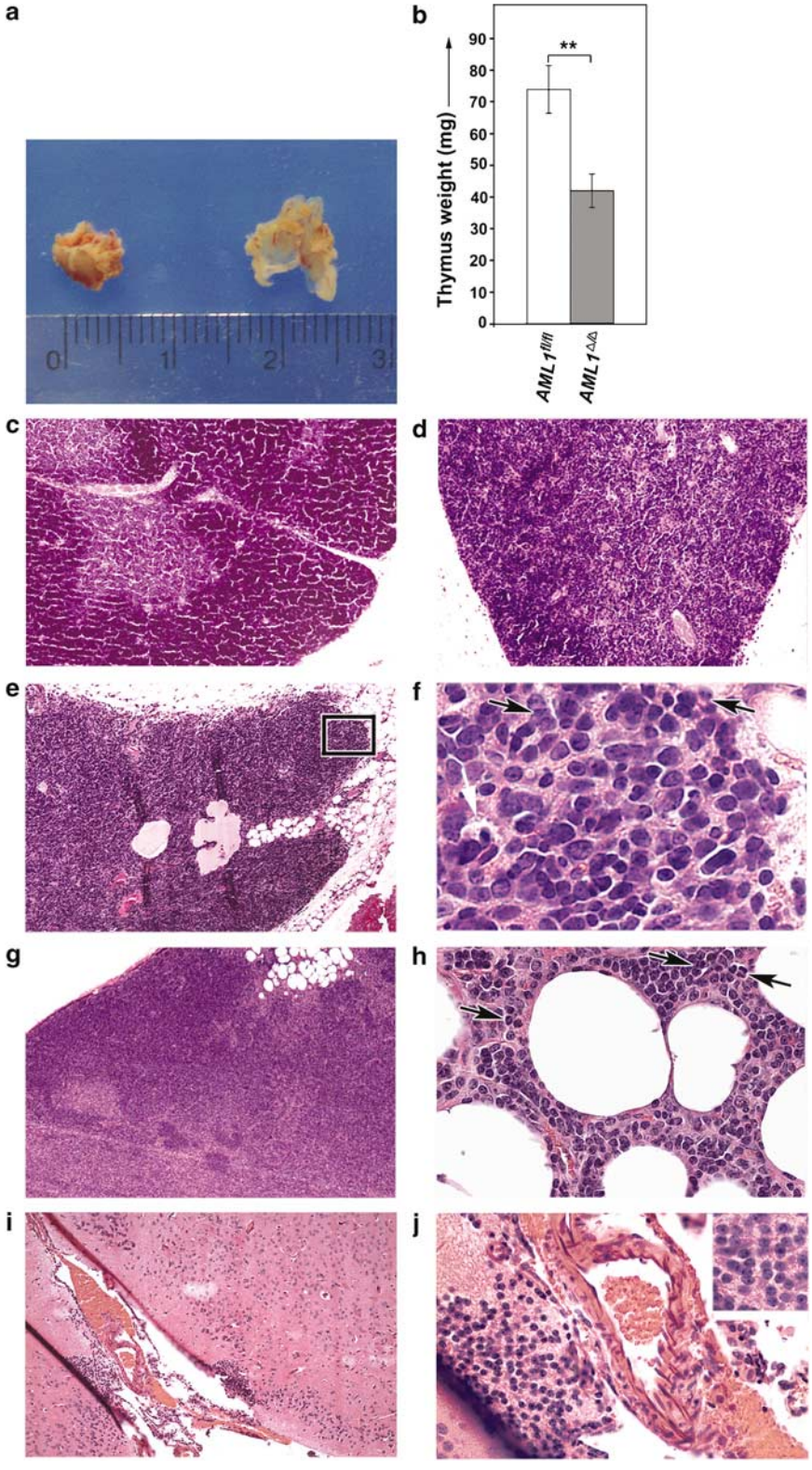

development of megakaryocytes and the terminal differentiation of T-lymphocytes. The short-term phenotypical changes in adult *AML1*$^{\Delta/\Delta}$ mice were surprisingly mild compared to the severe defects of *AML1* mutations during embryogenesis. In contrast, at longer latency, mice developed progressive splenomegaly due to the enlargement of the red pulp compartment resulting from myelomonocytic cell expansion. The white pulp compartment was decreased in size with a relatively reduced population of lymphoid cells. The enlargement of the spleen led to splenic hypofunction, accompanied by the presence of Howell-Jolly bodies in erythrocytes of the peripheral blood. The association of splenomegaly and functional hyposplenism is rare. We suggest that the observed functional hyposplenism is due to an immaturity of the splenic macrophages.

According to the Bethesda proposal of classification of nonlymphoid hematopoietic neoplasms in mice (Kogan *et al*., 2002), we observed a myelodysplastic syndrome. Criteria for diagnosis were thrombocytopenia without leukocytosis or erythrocytosis, together with dysplastic megakaryocytes, and the exclusion of a nonlymphoid leukemia. In human myelodysplastic syndromes a multistep progression to AML is documented by serial acquisition of cytogenetic abnormalities associated with progression of disease (Hirai *et al*., 1987; Hirai *et al*., 1988; Rowley, 1998). Splenomegaly has been reported in MDS-AML patients (Bourgeois *et al*., 2001). The finding of splenomegaly in our mice, might, therefore, indicate a commencing progression of the myeloid dysplasia. Further investigation of *AML1*$^{\Delta/\Delta}$ mice during late stages of adulthood will show whether preleukemic mice finally will develop a type of leukemia.

The observation of smaller thymuses, which mainly contained immature DN thymocytes, indicate a block in T-cell maturation and explain lymphocytopenia in the peripheral blood. These results are in accordance to Ichikawa *et al*. (2004), who found no reconstitution of thymocytes in recipients of a competitive repopulation assay, suggesting a block in T-cell maturation. Concluding from our detailed analysis of thymus cellularity and architecture in *AML1*$^{\Delta/\Delta}$ mice; however, we do not hypothesize an accumulation of precursors in the thymus, but rather the apoptosis of thymocytes prior to maturation. The observation of a reduction of the total number of thymocytes goes along with results from a conditional *AML1* knockout under control of the T-cell specific *lck*-Cre promoter. In this study, however, the dramatic shift from DP to DN thymocytes, which we observed in *AML1*$^{\Delta/\Delta}$ mice, had not been documented (Taniuchi *et al*., 2002). In contrast, Taniuchi *et al*. (2002) reported the requirement of *AML1* for CD4 repression in DN thymocytes. These discrepancies might appear, because *lck*-Cre expression becomes evident at a relatively late stage of development of immature DN thymocytes, while *Mx-Cre* expression reveals the effects of lacking AML1 at earlier stages of thymocyte development. In three of six *AML1*$^{\Delta/\Delta}$ mice studied in detail, prelymphomas or lymphomas originated in the thymus or in peripheral lymph nodes and metastasized to the liver or the brain. With our mouse model, we show that AML1 plays an important role in the control of hematopoietic cell maturation in adult mice, and that the lack of AML1 in hematopoietic cells leads to a defective architecture and function of hematopoietic organs and, at longer latency, to lymphoid neoplasms.

Haploinsufficiency of murine *AML1* was characterized by a slight reduction of the number of platelets in the peripheral blood of 15%, compared to a 50% reduction in *AML1*$^{\Delta/\Delta}$ mice. No abnormalities were detected in the number of myeloid and lymphoid cells in the periperal blood or spleen of *AML1* haploinsufficient mice (Sun and Downing, 2004). The different phenotypes are suggesting that expression of 50% of the normal amount of AML1 is sufficient to regulate myeloid cell proliferation and lymphoid cell differentiation, but not to compensate for defective megakaryopoiesis.

The defects of *AML1* deletion in adult mice also varied from those observed in the AML/ETO translocation. Although *in vitro* growth characteristics of multilineage hematopoietic progenitors were altered in mice lacking *AML1*, apparent in an increased self-renewal capacity (Ichikawa *et al*., 2004), *AML1*-deficiency did not lead to the immortalization of myeloid progenitors, observed in AML/ETO expressing cells (Okuda *et al*., 1998; Rhoades *et al*., 2000; Yuan *et al*., 2001; Higuchi *et al*., 2002). Also thrombocytopenia and mild lymphocytopenia seem to be characteristic for the loss of

Figure 5 Neoplastic progression to metastatic lymphomas. (**a**) Altered structure and size of the thymus in *AML1*$^{\Delta/\Delta}$ mice (left) compared to *AML1*$^{fl/fl}$ mice (right). (**b**) The thymus weight is significantly decreased in *AML1*$^{\Delta/\Delta}$ mice ($n=14$) compared to *AML1*$^{fl/fl}$ mice ($n=13$). **c-f**: Histopathology of the thymic lesions. (**c**) Thymus of a healthy *AML1*$^{fl/fl}$ mouse (H&E, original magnification $\times 100$). The distinction between the cortex and the medulla can be easily seen. (**d**) Atypical hyperplasia reduces the cortical/medullary distinction but is confined to the thymus (H&E, $\times 100$). (**e**) Thymic lymphoma (H&E, $\times 100$). A mixed cell population of immature lymphoid cells extends beyond the thymic capsule. Large pink thymic cysts as seen in the center occur sporadically in normal mice (Fredrickson and Harris, 2000). (**f**) At higher power, lymphoblasts, mixed with few cortical lymphocytes and apoptotic bodies are seen at the invasion front (H&E, $\times 400$, zoom factor 1.6). Some lymphoblasts contain a central, round nucleolus. At the left edge, a large tingible body macrophage (white arrow) containing phagocytosed apoptotic tumor cells, and reflecting high rates of cell proliferation and cell death, is seen (starry sky appearance). The black arrows point at numerous mitotic figures. (**g**) Lymphoblastic lymphoma of an enlarged cervical lymph node (H&E, $\times 50$). The neoplastic cells destroy the architecture of the lymph node and extend beyond its capsule into the adjacent fat tissue. (**h**) Higher power (H&E, $\times 400$, zoom factor 1.6) revealed that the lymphoma cells formed sheets of uniform medium-sized cells with round nuclei, a fine chromatine structure, a prominent central nucleolus or small scattered nucleoli, and a high mitotic rate (arrows: mitotic figures). (**i**) Metastases of the lymphoma shown in (h) to the meninges and the brain (H&E, $\times 50$). (**j**) Starting perivascular, the lymphoblasts diffusely infiltrate the brain cortex (H&E, $\times 400$). The vessel wall appears intact. The hemorrhage into the liquor occurred perimortally. The inset shows a similar cytology as in (**h**).

AML1, whereas no abnormalities were found in the blood cell counts of mice with the translocation (Higuchi *et al*., 2002). While we could show that the lack of AML1 in the hematopoietic system affected the structure and function of the spleen and the thymus, no histological abnormalities were found in any of the hematopoietic organs in conditional AML/ETO knock-in mice where AML/ETO expression was driven off of the endogenous AML1 regulatory sequences (Higuchi *et al*., 2002). In contrast, splenomegaly with an increase of immature myeloid populations as well as the development of lymphomas were described in leukemic AML/ETO mice after ENU treatment (Yuan *et al*., 2001). Thus, with the AML1 deletion, we are able to dissect the role of AML1 from the dominant-negative effects of the AML-ETO fusion protein and from effects caused by altered ETO expression.

Altogether, our mouse model is a valuable tool to study the role of AML1 in the adult mouse and to investigate the mechanisms underlying the development and progression of myelodysplastic syndromes. The conditional *AML1* knockout allele enables us to study what cooperative events support the development of AML1-related hematopoietic neoplasms.

Materials and methods

Generation of transgenic mice
The *AML1* targeting construct (Figure 1a) was generated by inserting a neomycin cassette flanked ('floxed') by loxP sites downstream of exon 5 of *AML1* and by inserting a loxP site upstream of exon 5 of the *AML1* gene. E14 embryonic stem (ES) cells were electroporated with the targeting construct and clones were selected. Genotyping was performed by PCR (Figure 1a and b, primers P3 + P4, see the Supplemental Materials link at the top of the online article). Correctly targeted ES cell clones were used for blastocyst injections; one chimera transmitted the targeted allele through the germline. Mice positive for the floxed *AML1* allele (*AML1*$^{fl/+}$) were obtained by breeding and crossed to each other on C57/BL6 × 129SvJ background. The offspring was screened for homozygosity (primers P1 + P2, P5 + P6). *AML1*$^{fl/fl}$ mice were then crossed to interferon-responsive *Mx-Cre* mice, and genotyped (primers P8 + P9, Supplemental Materials). Cre-mediated site-specific recombination of the loxP cassettes was induced by three intraperitoneal injections of 300 μg Poly-IPolyC (Sigma Aldrich Chemie GmbH, Taufkirchen, Germany) in 2–4 months old *AML1*$^{fl/fl}$ mice at two-day intervals (Kuhn *et al*., 1995). *AML1*$^{fl/fl}$ mice lacking the *Cre* gene were treated the same way and used as control mice. All animal experiments were conducted in a licensed animal facility in accordance with the German Animal Welfare Act (Tierschutzgesetz), following the guidelines of the European Convention for the Protection of Vertebrate Animals Used for Experimental and Other Scientific Purposes (1986). Mice were kept under specific pathogen-free conditions. Serological testing for viruses was negative.

Genotype analysis
Mice were genotyped by PCR to detect both the wild-type and alleles of the *AML1* targeting construct. Genomic DNA was isolated from tail biopsies and subjected to PCR primers (primers P1 + P2, P3 + P4, P5 + P6, P8 + P9, Supplemental Materials). PCR products were resolved by agarose gel electrophoresis. To test for recombination in murine tissue, DNA of peripheral blood, BM, spleen, liver, kidney and thymus was isolated by phenol chloroform extraction and genotyped by PCR analyses (triple primer PCR assay with primers P5 + P6 + P7).

Flow cytometry analysis
FACS analysis and cell sorting were performed using the BD FACSAria Cell-Sorting System. Murine spleen and BM cells were stained with rat anti-mouse Sca-1 (Ly6A/E), CD117 (c-Kit), Prominin-1 (13A4), CD4 (L3T4), CD8 (Ly-2), B220 (CD45R), IgM, Gr-1 (Ly6G), CD11b (Mac1). All cells were blocked with purified rat anti-mouse CD16/CD32 monoclonal antibody (Mouse BD Fc Block). As isotype control, we used R-Phycoerythrin-conjugated rat $IgG_{2a,\kappa}$ monoclonal immunoglobulin isotype control, Fluorescein Isothiocyanate-conjugated rat $IgG_{2b,\kappa}$ monoclonal immunoglobulin isotype control, and PE-Cy5-conjugated rat $IgG_{2a,\kappa}$ monoclonal immunoglobulin isotype control. Antibodies, except for Prominin-1, were purchased from BD Biosciences Pharmingen (Erembodegem, Belgium) and are listed in the Supplemental Materials link. Prominin-1 was ordered from eBioscience (San Diego, CA, USA). For lineage depletion of BM cells the Miltenyi Lineage Cell Depletion Kit (#130-090-858) was used, followed by Magnetic separation with Miltenyi MACS LS Columns and MACS Separator (Miltenyi Biotec, Bergisch Gladbach, Germany). FACS analysis was done on multiple mice (for details see Supplemental Materials link). Figures show mice representative for the analysis.

Hematological analysis
Peripheral blood was withdrawn from mice via saphenous vein puncture and collected in tubes containing EDTA. Complete blood counts were performed weekly using the HEMAVET HV 850FS analyzer (CDC Technologies, Oxford, CT, US). Cells were stained by using the Pappenheim method (May-Grünwald/Giemsa-stain), Peroxidase, and Alpha-naphthyl acetate esterase stain. Counts of erythrocytes containing Howell-Jolly bodies were performed by counting $\geqslant$1000 erythocytes per investigated mouse.

Histologic and immunohistochemical analysis
At various time-points after PolyIPolyC injections, mice were sacrificed by CO_2 asphyxiation. Selected organs, including spleen, thymus and BM were removed. Complete necropsies with emphasis on the hematopoietic system were performed in six *AML1*$^{\Delta/\Delta}$ mice and six *AML1*$^{fl/fl}$ control mice matched for age, sex and PolyI-PolyC-injection time. For a determination of organ size, organs were trimmed of fat and connective tissues and weighed. Tissues processed for microscopic evaluation were fixed in 10% neutral-buffered formalin, embedded in paraffin, sectioned (4-mm sections), mounted on slides and stained with hematoxylin and eosin. Goldner's trichrome staining was performed as previously described (Schiering *et al*., 1999). Bone was decalcified using Ossa fixona (Waldeck GmbH, Munster, Germany). Metachromatic mast cell granula were visualized by Toluidine blue staining.

For immunohistochemistry, frozen spleen fragments were embedded in Tissue-tek medium (Science Services, Munich, Germany), cut, air-dried, fixed in acetone or methanol, washed in PBST containing 0.1% Tween 20, and blocked with 2% BSA. Sections were incubated with purified anti-CD4 (L3T4), anti-B220 (CD45R), anti-Gr1 (Ly6G), or anti-CD11b (Mac1) from BD Biosciences PharMingen, followed by Cy3 AffiniPure F(ab″)2 Frag Donkey Anti-Rat IgG (Jackson Immuno-

Research, Cambridgeshire, UK), or Alexa Fluor 488 donkey anti-rat IgG (Molecular Probes Europe, Goettingen, Germany). Immmunohistochemistry was done on several mice. Details are available in the Supplemental Materials link. Figures show mice representative for the analysis.

Statistical analysis
The Student's *t*-test was used to determine the statistical differences between various experimental and control groups. The difference was considered statistically significant when $*P < 0.05$ or $**P < 0.01$.

Acknowledgements

We thank Roland Naumann, Maxi Oelsner, Sigrid Balschukat, Irena Konstantinova, and the Department of Internal Medicine I of the Carl Gustav Carus University Hospital Dresden for providing technical assistance, Jussi Helppi, Anke Muench-Wuttke, and Anja Klieman for biomedical services. Thanks also to Ralf Kittler, Carol Stocking and Joerg Cammenga for scientific discussion. We are grateful to Dennis Corbeil for providing us with the Prominin-1 antibody. This study was supported by the Max Planck Society, the Deutsche José Carreras Leukaemie-Stiftung e.V., and the Deutsche Forschungsgemeinschaft (SFB 655 and BA1433/4-2).

Note added in proof

While this manuscript was under review, Growney *et al*. (2005) reported that the loss of Runx1 perturbs adult hematopoiesis and is associated with a myeloproliferative phenotype. See Growney JD, Shigematsu H, Li Z, Lee BH, Adelsperger J, Rowan R et al. (2005). Blood 106: 494–504.

References

Bourgeois E, Caulier MT, Rose C, Dupriez B, Bauters F, Fenaux P. (2001). *Leukemia* **15**: 950–953.
Buchholz F, Refaeli Y, Trumpp A, Bishop JM. (2000). *EMBO Rep* **1**: 133–139.
Dunnick JK, Hardisty JF, Herbert RA, Seely JC, Furedi-Machacek EM, Foley JF *et al*. (1997). *Toxicol Pathol* **25**: 533–540.
Fredrickson TN, Harris AW. (2000). *Atlas of Mouse Hematopathology*. Harwood Academic Publishers: Amsterdam.
Higuchi M, O'Brien D, Kumaravelu P, Lenny N, Yeoh EJ, Downing JR. (2002). *Cancer Cell* **1**: 63–74.
Hirai H, Kobayashi Y, Mano H, Hagiwara K, Maru Y, Omine M *et al*. (1987). *Nature* **327**: 430–432.
Hirai H, Okada M, Mizoguchi H, Mano H, Kobayashi Y, Nishida J *et al*. (1988). *Blood* **71**: 256–258.
Ichikawa M, Asai T, Saito T, Yamamoto G, Seo S, Yamazaki I *et al*. (2004). *Nat Med* **10**: 299–304.
Imai Y, Kurokawa M, Izutsu K, Hangaishi A, Takeuchi K, Maki K *et al*. (2000). *Blood* **96**: 3154–3160.
Kogan SC, Ward JM, Anver MR, Berman JJ, Brayton C, Cardiff RD, *et al*., Hematopathology subcommittee of the Mouse Models of Human Cancers Consortium. (2002). *Blood* **100**: 238–245.
Kuhn R, Schwenk F, Aguet M, Rajewsky K. (1995). *Science* **269**: 1427–1429.
Lagasse E, Weissman IL. (1996). *J Immunol Methods* **197**: 139–150.
Lenny N, Meyers S, Hiebert SW. (1995). *Oncogene* **11**: 1761–1769.
Levanon D, Negreanu V, Bernstein Y, Bar-Am I, Avivi L, Groner Y. (1994). *Genomics* **23**: 425–432.
Lorsbach RB, Moore J, Ang SO, Sun W, Lenny N, Downing JR. (2004). *Blood* **103**: 2522–2529.
Michaud J, Scott HS, Escher R. (2003). *Cancer Invest* **21**: 105–136.
Miller JD, Stacy T, Liu PP, Speck NA. (2001). *Blood* **97**: 2248–2256.
Morohashi K, Tsuboi-Asai H, Matsushita S, Suda M, Nakashima M, Sasano H *et al*. (1999). *Blood* **93**: 1586–1594.
North T, Gu TL, Stacy T, Wang Q, Howard L, Binder M *et al*. (1999). *Development* **126**: 2563–2575.
Ogawa E, Inuzuka M, Maruyama M, Satake M, Naito-Fujimoto M, Ito Y *et al*. (1993a). *Virology* **194**: 314–331.
Ogawa E, Maruyama M, Kagoshima H, Inuzuka M, Lu J, Satake M *et al*. (1993b). *Proc Natl Acad Sci USA* **90**: 6859–6863.
Okuda T, Cai Z, Yang S, Lenny N, Lyu CJ, van Deursen JM *et al*. (1998). *Blood* **91**: 3134–3143.
Okuda T, van Deursen J, Hiebert SW, Grosveld G, Downing JR. (1996). *Cell* **84**: 321–330.
Osato M, Asou N, Abdalla E, Hoshino K, Yamasaki H, Okubo T *et al*. (1999). *Blood* **93**: 1817–1824.
Preudhomme C, Warot-Loze D, Roumier C, Grardel-Duflos N, Garand R, Lai JL *et al*. (2000). *Blood* **96**: 2862–2869.
Rhoades KL, Hetherington CJ, Harakawa N, Yergeau DA, Zhou L, Liu LQ *et al*. (2000). *Blood* **96**: 2108–2115.
Roumier C, Fenaux P, Lafage M, Imbert M, Eclache V, Preudhomme C. (2003). *Leukemia* **17**: 9–16.
Rowley JD. (1998). *Annu Rev Genet* **32**: 495–519.
Schiering A, Menschikowski M, Mueller E, Jaross W. (1999). *Atherosclerosis* **144**: 73–78.
Silva FP, Morolli B, Storlazzi CT, Anelli L, Wessels H, Bezrookove V *et al*. (2003). *Oncogene* **22**: 538–547.
Song WJ, Sullivan MG, Legare RD, Hutchings S, Tan X, Kufrin D *et al*. (1999). *Nat Genet* **23**: 166–175.
Steensma DP, Gibbons RJ, Mesa RA, Tefferi A, Higgs DR. (2005). *Eur J Haematol* **74**: 47–53.
Sun W, Downing JR. (2004). *Blood* **104**: 3565–3572.
Taketani T, Taki T, Takita J, Tsuchida M, Hanada R, Hongo T *et al*. (2003). *Genes Chromosomes Cancer* **38**: 1–7.
Taniuchi I, Osato M, Egawa T, Sunshine MJ, Bae SC, Komori T *et al*. (2002). *Cell* **111**: 621–633.
Wang Q, Stacy T, Binder M, Marin-Padilla M, Sharpe AH, Speck NA. (1996a). *Proc Natl Acad Sci USA* **93**: 3444–3449.
Wang Q, Stacy T, Miller JD, Lewis AF, Gu TL, Huang X *et al*. (1996b). *Cell* **87**: 697–708.
Wang SW, Speck NA. (1992). *Mol Cell Biol* **12**: 89–102.
Yergeau DA, Hetherington CJ, Wang Q, Zhang P, Sharpe AH, Binder M *et al*. (1997). *Nat Genet* **15**: 303–306.
Yin AH, Miraglia S, Zanjani ED, Almeida-Porada G, Ogawa M, Leary AG *et al*. (1997). *Blood* **90**: 5002–5012.
Yuan Y, Zhou L, Miyamoto T, Iwasaki H, Harakawa N, Hetherington CJ *et al*. (2001). *Proc Natl Acad Sci USA* **98**: 10398–10403.

Supplementary Information accompanies the paper on Oncogene website (http://www.nature.com/onc).